Polymer-based thermo-optic waveguide beam deflector with novel dual folded-thin-strip heating electrodes

Jin-Ha Kim
Lin Sun
Chiou-Hung Jang
Chul-Chae Choi
Ray T. Chen, FELLOW SPIE
University of Texas at Austin
Department of Electrical and Computer Engineering
10100 Burnet Road, PRC/MER R9900
Austin, Texas 78758
E-mail: raychen@uts.cc.utexas.edu

Abstract. A new design scheme for a polymeric waveguide thermo-optic beam deflector is presented and experimentally demonstrated. The refractive indices of the waveguide materials can be thermally tuned by applying electric current through a metal thin film electrode deposited and patterned using standard lithography on top of the waveguide. In doing so, the geometry of the electrode determines the performance and reliability of the beam deflector. We form a pair of heating electrodes sitting opposite to each other like interlocked sawteeth that have a folded-thin-strip substructure, and hence demonstrate an advanced beam deflector that has biangular sweeping capability, low power consumption, less wavefront distortion, and high reliability. A full sweep angle of 56.5 mrad (3.24 deg) and 1×8 switching capability at a 1550 nm wavelength are attained with an average power consumption of 247 mW per switching between adjacent resolvable spots. Switching from the zero-bias spot to the first resolvable spot exhibits a response time of 2 ms in both rising and falling. [DOI: 10.1117/1.1534594]

Subject terms: beam deflectors; integrated optics; optical switches; optical waveguides; polymers; thermo-optic effects.

Paper 020173 received May 2, 2002; revised manuscript received Aug. 6, 2002; accepted for publication Jul. 31, 2002.

1 Introduction

Thermo-optic laser beam deflectors implemented in polymeric planar waveguides have potential applications in integrated optics as switching elements, when incorporated with proper collimating and focusing elements. Waveguide thermo-optic beam deflectors based on prism-array-shaped refractive index modulation have been reported to be feasible candidates to this application.[1,2] Although their electro-optic counterparts[3–7] have possibly much faster operating speed, they have certain drawbacks such as high driving voltage, decay of the electro-optic coefficient, polarization dependency, and complex fabrication process. On the other hand, low power operation and a large deflection angle can be easily achieved by thermo-optic beam deflection technique in polymeric waveguides due to the fact that polymers possess a high thermo-optic coefficient ($\sim 10^{-4}/°C$) and low thermal conductivity (0.1 to 0.3 W/mK). Moreover, the thermo-optic effect is an inherently polarization-independent process, which enables polarization-independent operation.

In our previous works, we used two different approaches to implement the thermo-optic beam deflector. The first utilized the difference of the thermo-optic coefficient between silica and polymer as the driving force of beam deflection.[1] However, combining two different material systems increased the complexity of the fabrication process and resulted in a scattering loss at the interfaces. The second adopted a prism-array-shaped heating electrode on top of a polymeric planar waveguide.[2] When the electrode is heated up in this type of device, the waveguide layers beneath the electrode have lowered refractive index profiles, resembling the shape of the electrode. This could be the most practical index modulation method for a thin film thermo-optic beam deflector, but because of its plain electrode design, which was an array of triangular plates connected to adjacent ones at their base, it had current bottlenecks resulting in a nonuniform heating pattern and oftentimes failure at the bottleneck points even at a low driving current.

In this paper, we report an improved design of the second type of beam deflector, which has lower power consumption and better reliability, as well as biangular beam sweeping capability. It incorporates dual folded-thin-strip heating electrodes, which cover the area of the desired prism arrays with tiny open areas between the strips. This new design helps achieve more uniform temperature distribution over the entire electrode area and improves power consumption and reliability by removing current bottlenecks. In addition, a pair of electrodes sitting opposite to each other like interlocked sawteeth enables a biangular sweep, while only a uniangular sweep is possible with the previous single-electrode design. The power budget per electrode in the dual-electrode configuration is also half that of a single-electrode deflector with the same maximum sweep angle. The schematic structure of the proposed device and a micrograph of the electrode are shown in Figs. 1(a) and 1(b), respectively.

 0091-3286/2003/$15.00

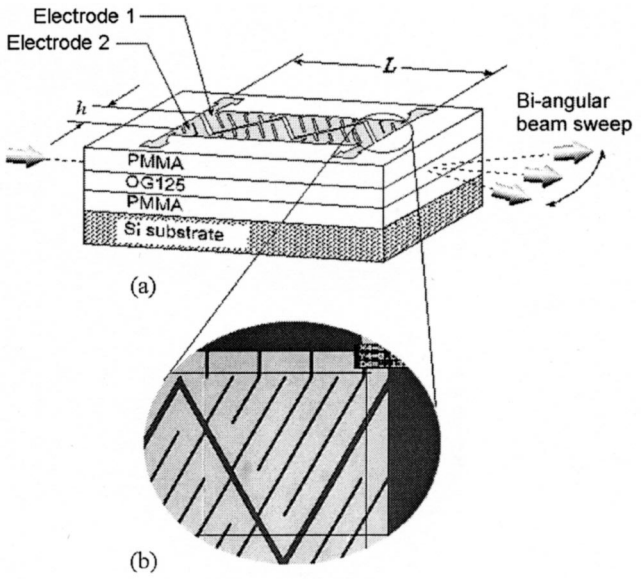

Fig. 1 (a) Schematic view of the beam deflector and (b) the micrograph of the top electrodes. The electrode has folded thin strip Al film of uniform width 80 μm. The outside dimensions of the beam deflecting part of the electrode are $h=660$ μm and $L=8400$ μm. The thickness of the core and the claddings are 5.2 and 5 μm, respectively.

2 Design Principle

An index-modulated prism array is equivalent to a medium with a linearly graded index distribution along the direction perpendicular to the beam propagation to a good approximation. Based on this, a minor geometrical calculation gives a complete description of the beam propagation in the beam deflector, making time-consuming simulations relatively unnecessary. Given an input beam in the ray optic limit entering the deflector at the center of the input aperture, the beam angle θ and the lateral position x are expressed as functions of the propagation distance z by the following equations:[6]

$$\theta=\frac{\Delta}{h}z, \tag{1}$$

$$x=\frac{\Delta}{2h}z^2, \tag{2}$$

where Δ is equal to $\Delta n/n_0$, the fractional change of the effective refractive index; and h is the height of the beam deflector. When designing a beam deflector, we must take into account a constraint that the beam should remain in the lateral boundaries until it reaches the output aperture. This constraint implies $x=h/2$ when $z=L$ at the maximum deflection condition. By applying the constraint to Eq. (2) and arranging it for L, we obtain the optimum modulation length:

$$L=\frac{h}{(\Delta_{\max})^{1/2}}. \tag{3}$$

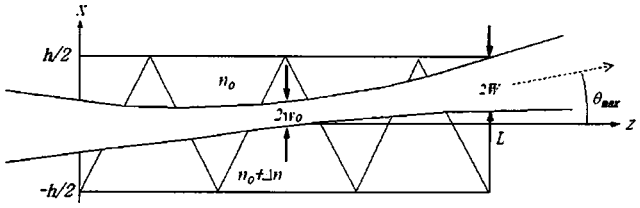

Fig. 2 Deflection of a Gaussian beam. The maximum deflection angle $\theta_{\max}$ is determined from the geometrical factors h and L and the beam size w_0 at the waist under the constraint that the deflected beam must not deviate over the lateral boundaries of the prism array region. Applying more electrical power beyond this limit would only degrade the output beam quality without substantially increasing the deflection angle. The Gaussian beam size W at the output apertures is given by $W=w_0[1+(\lambda_0 L/2\pi n_0 w_0^2)^2]^{1/2}$.

Finally, the maximum beam deflection angle is found by combining Eqs. (3) and (1) with $z=L$, as given next.

$$\theta_{\max}=(\Delta_{\max})^{1/2}=\frac{h}{L}. \tag{4}$$

This result should be interpreted such that the maximum achievable deflection angle is determined by either the square root of the maximum index modulation $(\Delta_{\max})^{1/2}$ or the geometry factor h/L, whichever is smaller; however, those two factors should match for an optimized design, as in Eq. (4).

In realistic cases, the finite beam width and the diffraction should also be taken into account. Since the thermo-optic effect usually provides a large enough index modulation at a moderate temperature tuning, we speculate in detail only on the geometric limit, with given h,L, and the Gaussian spot size w_0 at the beam waist. Suppose a Gaussian beam passing through the deflector with its waist at the center of the deflector is under deflection, as shown in Fig. 2. With the constraint that the deflected beam must remain in the prism array until it reaches the output aperture, the maximum deflection angle $\theta_{\max}$ is expressed by

$$\theta_{\max}=\frac{h}{L}\left\{1-\frac{2w_0}{h}\left[1+\left(\frac{\lambda_0 L}{2\pi n_0 w_0^2}\right)^2\right]^{1/2}\right\}, \tag{5}$$

where λ_0 is the vacuum wavelength of the light. Note that the full sweep angle is $2\theta_{\max}$ since the beam scans between $\theta_{\max}$ and $-\theta_{\max}$.

A wide sweep angle generally means a good beam deflector, but it cannot be an objective measure of beam deflector performance without consideration of the beam divergence. The most widely used figure of merit with regard to beam deflectors is the number of resolvable spots defined by the maximum deflection angle divided by the beam divergence angle, $M=\theta_{\max}/\theta_{\mathrm{div}}$ (Ref. 8). Here, θ_{div} of a Gaussian beam is given by

$$\theta_{\mathrm{div}}=\frac{\lambda_0}{\pi n_0 w_0}. \tag{6}$$

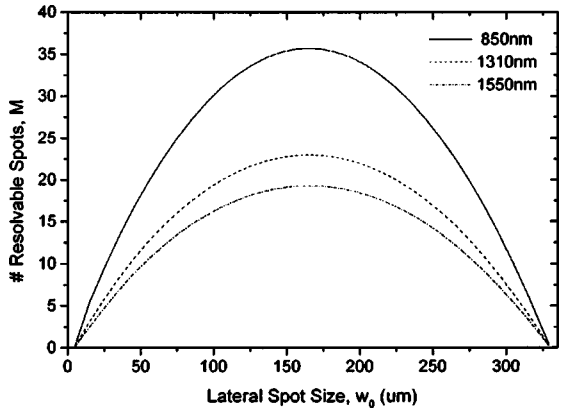

Fig. 3 Number of resolvable spots as a function of lateral spot size w_0 at $\lambda_0 = 850$, 1310, and 1550 nm: $h = 660$ μm and $L = 8400$ μm were assumed for calculation. The most efficient beam deflector is obtained with the beam width $2w_0$ equal to half of the deflector width h.

However, in terms of optical switching, the maximum number of output channels N should be counted by $M+1$, for M means the number of resolvable spots other than the original undeflected spot that counts for 1.

The beam deflector reported in this paper has a pair of prism array-shaped electrodes of height 700 μm and length 8400 μm interlocked with a gap of 40 μm, resulting in $h = 660$ μm effectively and $L = 8400$ μm. The number of resolvable spots M calculated from Eqs. (5) and (6) is depicted in Fig. 3 as a function of w_0 at three different wavelengths. It is interesting to note that M is maximized when the beam width $2w_0$ is a half of the beam deflector height h.

3 Fabrication

We consecutively spin-coated PMMA/OG125/PMMA layers on silicon substrate to build a planar waveguide structure. OG125 is a UV-curing resin from Epoxy Technology, Inc. The refractive index was measured to be 1.484 at 1.3 μm after curing and baking. PMMA (poly-methyl methacrylate) used as cladding material has refractive index of 1.479 at 1.3 μm. Though the device was to be tested at 1.55 μm, the indices were measured at only 1.3 μm because the prism coupler used for the measurement was not equipped with a 1.55-μm light source. Nevertheless, the index difference between the core and the cladding would be approximately the same even if they were measured at 1.55 μm. The thickness of core and bottom and top cladding are 5.2, 5, and 5 μm, respectively. This combination of layers makes a single-mode planar waveguide with the cutoff wavelength of 1.22 μm. On top of the waveguide, 200-nm-thick aluminum film was deposited by *e*-beam evaporation and patterned into a pair of folded-thin-strip electrodes by standard photolithography and wet etch process. The width of the strip is 80 μm and the gap between adjacent strips is 7 μm, which is designed relatively small compared to the strip width and the waveguide thickness to minimize unwanted index variation in the gap region. The resistances of electrodes 1 and 2 were measured to be 338 and 332 Ω, respectively. Finally, the sample was cleaved and polished at both of its end faces.

4 Device Characteristics

In the experiment, a fiber-pigtailed 1550 nm distributed feedback (DFB) LD was used for device characterization. The Gaussian-like laser output at the end of the fiber, of which the mode field diameter is about 11 μm, was focused into a spot with an enlarged radius of 133 μm with a microscope objective lens. The lateral spot size was measured by the scanning knife-edge method before the device was placed on its position, and turned out to be a little smaller than the optimized value that was suggested by the graph in Fig. 3. The beam was again vertically squeezed to achieve mode-match to the waveguide mode with a rod lens that had focal length of 1.027 mm. The output beam had high divergence in the vertical direction, therefore another rod lens with a focal length of 1.719 mm was used to reduce the divergence to a desired amount. A screen was placed 254 mm from the center of the device, and an IR vidicon camera captured the beam pattern on the screen to determine the beam position. For precise measurement of the

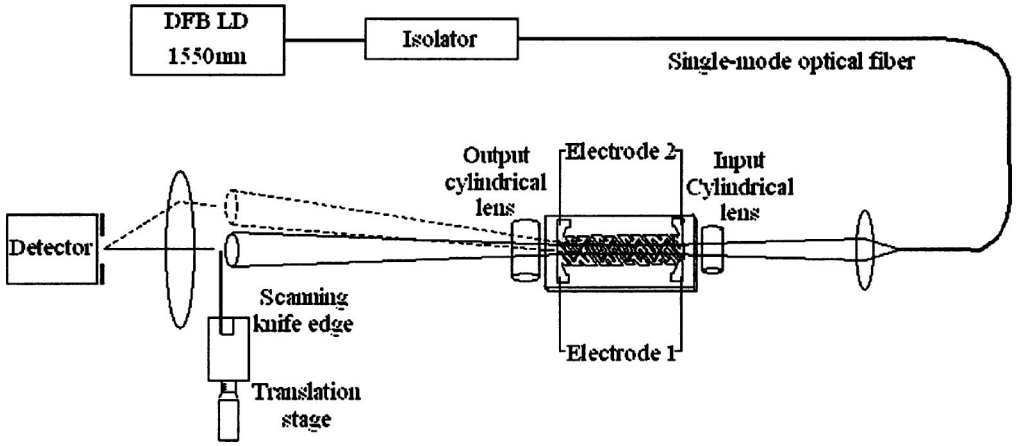

Fig. 4 Experimental setup for the beam deflector characterization. The output beam profile is precisely measured by scanning knife-edge method. A screen can be alternatively placed at the knife-edge position to measure beam position as a function of applied electrical power through an IR vidicon camera.

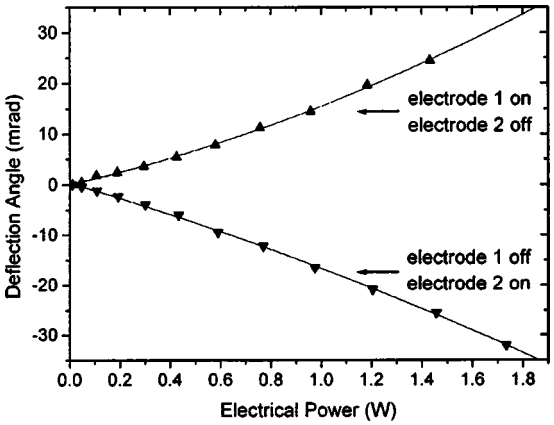

Fig. 5 Beam deflection angle as a function of applied electrical power. The upper curve represents deflection with electrode 1, and the lower curve represents deflection with electrode 2, in opposite directions from each other.

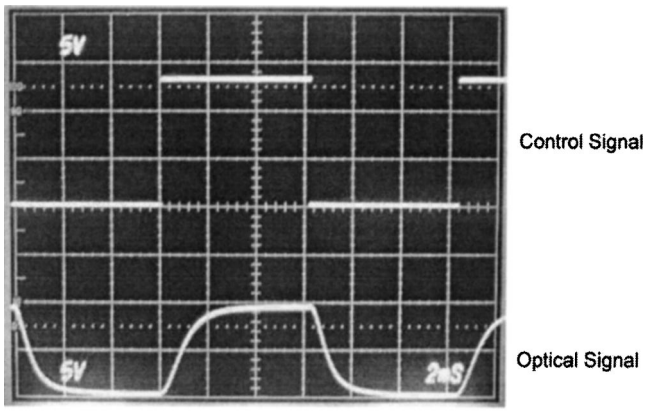

Fig. 7 Response of the beam deflector (lower trace) to the square input pulse (upper trace). Switching from the zero-bias spot to the first resolvable spot exhibits response time of 2 ms in both rising and falling.

lateral beam divergence angle, we again used the knife-edge scanning method at the screen position, as shown in Fig. 4.

The deflection angle as a function of applied electrical power is shown in Fig. 5. The maximum deflection angle that can be measured without significant beam distortion is 24.4 mrad with electrode 1 and 32.1 mrad with electrode 2, adding up to full sweep angle of 56.5 mrad (3.24 deg). Since the index change is proportional to the temperature change and the temperature change is proportional to the generated heat, it is natural to expect a linear relation between the deflection angle and the applied electrical power. But as shown in the graph, a slight deviation from linear relation is observed. The electrical power required to drive the deflector turned out to be only about 13% of that of Ref. 2. This improvement can be attributed to the new electrode design.

The angular distribution of the output beam was measured as a function of the deflection angle with electrode 2 in operation, and was fitted with Gaussian curves. The result is shown in Fig. 6. We can see from the graph that the beam divergence increases as the deflection angle does. We believe this is mainly because of the fact that the index distribution does not exactly resemble the shape of the electrode; also, particles imbedded in the end faces, which are due to the polishing process, scatter light, further broadening the beam. Therefore, the practical operation range of the deflection angle is limited to less than half of the maximum angle estimated from Eq. (5), as is the number of resolvable spots. The practical value of the number of resolvable spots M is approximately 7 for this device, which implies the capability of being a 1×8 optical switch.

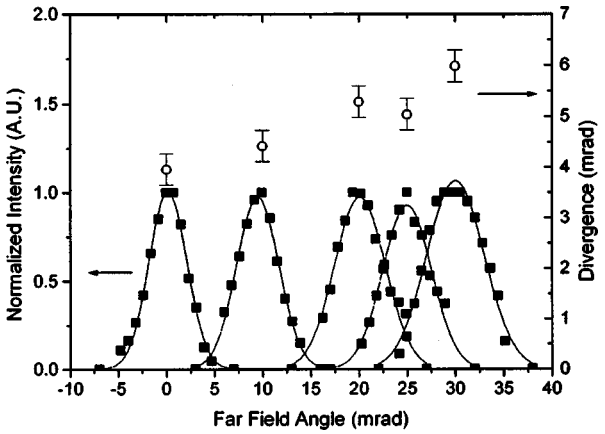

Fig. 6 Gaussian-fitted far-field distribution (solid square and solid line) and the divergence angle (hollow circle with error bar) of the deflected beam at a few selected deflection angles with electrode 2 in operation.

The switching time between the zero-bias spot and the first resolvable spot was evaluated. We placed a knife-edge between the two spot positions, blocking the zero-bias spot. A photodetector was placed behind the first resolvable spot position. The beam control signal and the photodetector signal are shown in the oscilloscope screen shown in Fig. 7. Both the rising and the falling times are 2 ms, which is a typical number for thermo-optic devices based on polymeric waveguides.

5 Conclusion

We demonstrated a polymeric waveguide thermo-optic beam deflector with an improved design. Full sweep angle of 56.5 mrad (3.24 deg) and 1×8 switching capability were attained with power consumption of 247 mW per switching between adjacent resolvable spots at a 1550 nm wavelength. The response time for switching from the zero-bias spot to the first resolvable spot was 2 ms. The results confirm the feasibility of the thermo-optic beam deflector to be a key component for the polymeric waveguide optical switch as well as for other beam-steering applications. Work is underway to incorporate the beam deflector with integrated waveguide total-internal-reflection mirrors as collimating and focusing elements to build $1\times N$ fiber optic switches.

Acknowledgments

This research was supported by the Air Force Office of Scientific Research, the Air Force Research Laboratory, the

Ballistic Missile Defense Organization, the Defense Advanced Research Projects Agency and the Advanced Technology Program of the state of Texas.

References

1. S. Tang, B. Li, X. Han, J. M. Taboada, C.-H. Jang, J.-H. Kim, L. Sun, and R. T. Chen, ''An integrated thin-film thermo-optic waveguide beam deflector,'' *Appl. Phys. Lett.* **76**, 2289–2292 (2000).
2. C.-H. Jang, L. Sun, J.-H. Kim, X. Lu, G. Karve, R. T. Chen, and J. J. Maki, ''A thin-film polymeric waveguide beam deflector based on thermooptic effect,'' *IEEE Photonics Technol. Lett.* **13**, 490–492 (2001).
3. J. F. Revelli, ''High-resolution electrooptic surface prism waveguide deflector: an analysis,'' *Appl. Opt.* **19**, 389–397 (1980).
4. Y. Chiu, D. D. Stancil, T. E. Schlesinger, and W. P. Risk, ''Electro-optic beam scanner in $KTiOPO_4$,'' *Appl. Phys. Lett.* **69**, 3134–3136 (1996).
5. K. T. Gahagan, V. Gopalan, J. M. Robinson, Q. X. Jia, T. E. Schlesinger, and D. D. Stancil, ''Integrated electro-optic lens/scanner in a $LiTaO_3$ single crystal,'' *Appl. Opt.* **38**, 1186–1190 (1999).
6. J.-H. Kim, L. Sun, C.-H. Jang, D. An, J. M. Taboada, Q. Zhou, X. Lu, R. T. Chen, B. Li, X. Han, S. Tang, H. Zhang, W. H. Steier, A. S. Ren, and L. R. Dalton, ''Polymetric waveguide beam deflector for electro-optic switching,'' *Proc. SPIE* **4279**, 37–44 (2001).
7. R. T. Chen, ''Polymer-based photonic integrated circuits,'' *Opt. Laser Technol.* **25**, 347–365 (1993).
8. A. Yariv, *Quantum Electronics*, 3rd ed., pp. 323–325, Wiley, New York (1989).

Biographies and photographs of the authors not available.